

# New Superconductivity Dome in $\text{LaFeAsO}_{1-x}\text{F}_x$ Accompanied by Structural Transition

J. Yang,<sup>1</sup> R. Zhou,<sup>1</sup> L. L. Wei,<sup>1</sup> H. X. Yang,<sup>1</sup> J. Q. Li,<sup>1</sup> Z. X. Zhao,<sup>1</sup> and Guo-qing Zheng<sup>1,2,\*</sup>

<sup>1</sup>*Institute of Physics and Beijing National Laboratory for Condensed Matter Physics,  
Chinese Academy of Sciences, Beijing 100190, P. R. China*

<sup>2</sup>*Department of Physics, Okayama University, Okayama 700-8530, Japan*  
(Dated: July 29, 2021)

High temperature superconductivity is often found in the vicinity of antiferromagnetism. This is also true in  $\text{LaFeAsO}_{1-x}\text{F}_x$  ( $x \leq 0.2$ ) and many other iron-based superconductors, which leads to proposals that superconductivity is mediated by fluctuations associated with the nearby magnetism. Here we report the discovery of a new superconductivity dome without low-energy magnetic fluctuations in  $\text{LaFeAsO}_{1-x}\text{F}_x$  with  $0.25 \leq x \leq 0.75$ , where the maximal critical temperature  $T_c$  at  $x_{opt} = 0.5 \sim 0.55$  is even higher than that at  $x \leq 0.2$ . By nuclear magnetic resonance and Transmission Electron Microscopy, we show that a C4 rotation symmetry-breaking structural transition takes place for  $x > 0.5$  above  $T_c$ . Our results point to a new paradigm of high temperature superconductivity.

PACS numbers: 74.25.nj, 74.70.Xa, 76.60.-k, 74.25.Ha

In conventional superconductors, the glue binding two electrons to form an electron pair (Cooper pair) is phonon, the quantization of lattice vibrations. In copper-oxide high temperature superconductors or heavy-fermion compounds, superconductivity emerges in the vicinity of antiferromagnetism, therefore it is believed by many that magnetic interactions (fluctuations) associated with the close-by magnetically-ordered phase mediate the electron pairing [1, 2]. Iron pnictides are a new class of high temperature superconductors [3, 4]. Carrier-doping by element substitution [3, 5–7] or oxygen defect [8] suppress the magnetic order and superconductivity appears. In the carrier-concentration range where superconductivity emerges, strong low-energy magnetic (spin) fluctuations survive [9–11]. This naturally leads to many proposals that superconductivity in the iron pnictides is also due to spin fluctuations associated with the nearby magnetic phase [12–14].

The prototype iron-pnictide  $\text{LaFeAsO}$  becomes superconducting when the magnetic order is suppressed upon replacing a part of oxygen (O) by fluorine (F). The superconducting transition temperature  $T_c$  forms a dome shape as a function of F-content, with the highest  $T_c = 27$  K at  $x = 0.06$  where strong low-energy spin fluctuations were found by nuclear magnetic resonance (NMR) measurements [10]; the F-content could not exceed 0.2 [3, 10, 15]. The high-pressure synthesis technique has proved to be powerful in making high F-concentration compounds [4], and the F-content was able to reach  $x = 0.6$  by this technique [16]. Recently, it was reported that, with high-pressure synthesis technique, hydrogen can also be doped to a high rate of  $x = 0.53$  [17]. In this work, we succeeded in synthesizing a series of high-doping samples of  $\text{LaFeAsO}_{1-x}\text{F}_x$  with  $0.25 \leq x \leq 0.75$  by high-pressure synthesis technique. The  $T_c$  forms a new dome shape peaked at  $x_{opt} = 0.5 \sim 0.55$  with a maximal  $T_c = 30$  K below which diamagnetism appears (the electrical resistivity starts to drop at  $T_c^0 \sim 40$  K). The

physical properties are completely different from the first dome. Over the entire new dome, there is no indication of low-energy magnetic fluctuations as evidenced by the spin-lattice relaxation rate ( $1/T_1$ ) divided by temperature ( $T$ ),  $1/T_1T$ . Instead, above the dome and for  $x > 0.5$ , we find a new type of phase transition below which a four-fold symmetry (C4 rotation symmetry) is broken.

The polycrystalline samples of  $\text{LaFeAsO}_{1-x}\text{F}_x$  (with nominal fluorine content  $x = 0.25, 0.3, 0.4, 0.5, 0.55, 0.6, 0.65, 0.7$  and  $0.75$ ) were prepared by the high pressure synthesis method. In the first step, the precursor LaAs powder was obtained by reacting La pieces (99.5%) and As powders (99.999%). In the second step, the starting materials LaAs, Fe (99.9%),  $\text{Fe}_2\text{O}_3$  (99.9%) and  $\text{FeF}_2$  (99.9%) were mixed together according to the nominal ratio and sintered in a six-anvil high-pressure synthesis apparatus under a pressure of 6 GPa at 1250°C for 2-4 hours. After sintering, the sample was quickly quenched to room temperature and then the pressure was released. This rapid quenching process was not used in the previous works [4, 16], but is important to keep the metastable phase which cannot be formed at ambient pressure.

Powder X-ray diffraction (XRD) with Cu  $K\alpha$  radiation were performed at room temperature to characterize the phase and structural parameters. The temperature dependence of resistivity were measured by a standard four-probe method. The  $T_c$  was determined by both DC susceptibility using a superconducting quantum interference device (Quantum Design) and AC susceptibility using an *in situ* NMR coil. For NMR measurements, the samples were crushed into fine powders with each grain's diameter less than  $50\mu\text{m}$ . The samples were then put in the magnetic field of 12 T at room temperature. Mechanical vibration was added to the sample so that the  $a$ -axis of the grains are aligned parallel to the magnetic field direction. The nucleus  $^{75}\text{As}$  has a nuclear spin  $I = 3/2$  and the nuclear gyromagnetic ratio  $\gamma = 7.2919$  MHz/T. The NMR spectra were obtained by

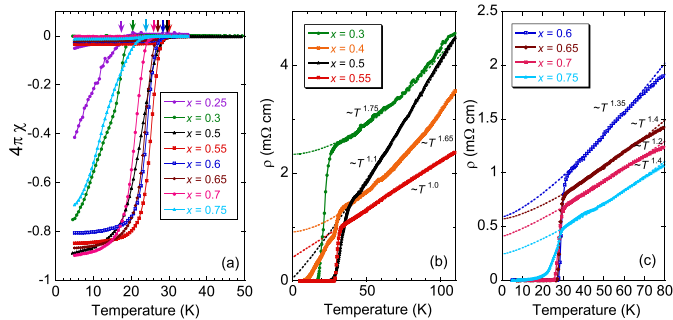


FIG. 1. The electrical resistivity and DC susceptibility of  $\text{LaFeAsO}_{1-x}\text{F}_x$ . (a) The DC susceptibility data measured with an applied magnetic field of 10 Oe. The arrows indicate the on-set temperature of the diamagnetism for each sample, which was defined as  $T_c$ . (b, c) The low temperature electrical resistivity. The dashed lines are the fittings to  $\rho(T) = \rho_0 + AT^n$  over the temperature range shown.

scanning the RF frequency and integrating the spin echo at a fixed magnetic field  $H_0$ . The spin-lattice relaxation time  $T_1$  was determined by using the saturation-recovery method. The nuclear magnetization  $M$  can be fitted to  $1 - M(t)/M(\infty) = 0.1\exp(-t/T_1) + 0.9\exp(-6t/T_1)$  expected for the central transition peak, where  $M(t)$  is the nuclear magnetization at time  $t$  after the single saturation pulse [18]. For TEM observations, a JEOL 2100F TEM equipped with cooling (below  $T=300$  K) or heating sample holders (above  $T=300$  K), was used for investigating the structural properties of these materials.

Figure 1(a) shows the DC susceptibility data. The  $T_c$  is defined as the onset of the diamagnetism in this paper, which reaches the highest value of 30 K at  $x = 0.55$ . The superconducting volume fractions of these samples, as shown in Fig. 1(a), indicate the bulk nature of the superconductivity, which was further assured by a clear decrease of  $^{75}\text{As}$  spin-lattice relaxation rate below  $T_c$  (see below). Figure 1(b)(c) show the temperature dependence of the electrical resistivity  $\rho$  for  $\text{LaFeAsO}_{1-x}\text{F}_x$  ( $0.3 \leq x \leq 0.75$ ). In the literatures, superconducting critical temperature was often defined as the temperature below which  $\rho$  starts to drop. In such a definition, the highest critical temperature is realized at  $x=0.5$  with  $T_c^p \sim 40$  K. The resistivity data can be fitted by the equation  $\rho = \rho_0 + AT^n$  (data over the whole temperature range, see ref. [19]). For a conventional metal described by Landau Fermi liquid theory, the exponent  $n = 2$  is expected. However, we find  $n < 2$  for all F-concentrations, which is suggestive of non-Fermi liquid behavior. Most remarkably, a  $T$ -linear behavior ( $n = 1$ ) is observed for  $x=0.5$  over the range of  $60 \text{ K} < T < 110 \text{ K}$ , and for  $x = 0.55$  over the range of  $33 \text{ K} < T < 140 \text{ K}$ . The evolution with Fluorine content  $x$  of the exponent  $n$ , which was obtained by a sliding power law, and  $T_c$  are shown in Fig. 2. Note that neither F-doping nor oxygen-deficiency was

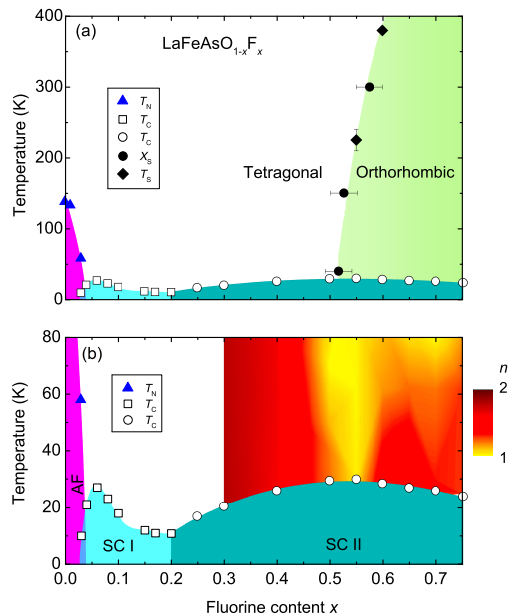


FIG. 2. The obtained phase diagram of  $\text{LaFeAsO}_{1-x}\text{F}_x$ . AF denotes the antiferromagnetically ordered phase, SC I and SC II denote the superconducting phases obtained by conventional solid-state and high-pressure synthesis methods, respectively. (a) Doping dependence of the magnetic ( $T_N$ ), superconducting ( $T_c$ ) and structural transition temperatures ( $T_s$ ). The  $T_N$  and  $T_c$  in SC I are taken from ref. [10]. The  $T_s$  for  $x = 0.55$  and  $0.6$  was obtained from NMR and TEM measurements, respectively.  $x_s$  is the critical F-concentration at which the structure transition takes place. (b) The evolution of the exponent  $n$  obtained by fitting the electrical resistivity to a relation  $\rho(T) = \rho_0 + AT^n$ .

able to go beyond  $x = 0.2$  in the past, and the superconductivity in the high-doping region is unprecedented.

The crystal symmetry transition is probed by measuring a change in the electric field gradient (EFG) tensors,  $V_{\alpha\alpha} = \frac{\partial^2 V}{\partial \alpha^2}$  ( $\alpha = x, y, z$ ), at the  $^{75}\text{As}$  and  $^{139}\text{La}$  sites, where  $V$  is the electrical potential. The EFG is related to the observables called nuclear quadrupole resonance (NQR) frequency tensors  $\nu_\alpha = \frac{eQ}{4I(2I-1)}V_{\alpha\alpha}$ , where  $I$  is the nuclear spin and  $Q$  is the nuclear quadrupole moment. Let us use the following EFG asymmetry parameter to describe the in-plane anisotropy.

$$\eta = \frac{\nu_x - \nu_y}{\nu_x + \nu_y} \quad (1)$$

When the four-fold symmetry exists in the  $ab$ -plane,  $V_{xx}=V_{yy}$  so that  $\eta = 0$ . When the four-fold symmetry is broken, then  $V_{xx}$  and  $V_{yy}$  are not identical so that  $\eta$  becomes finite. By  $^{75}\text{As}$  NMR and  $^{139}\text{La}$  nuclear quadrupole resonance (NQR), We find that  $\eta$  changes from 0 to a finite value below the structural transition temperature  $T_s = 40\sim 380$  K for compounds with  $x > 0.5$ . Figure 2(a) shows the phase diagram that depicts the

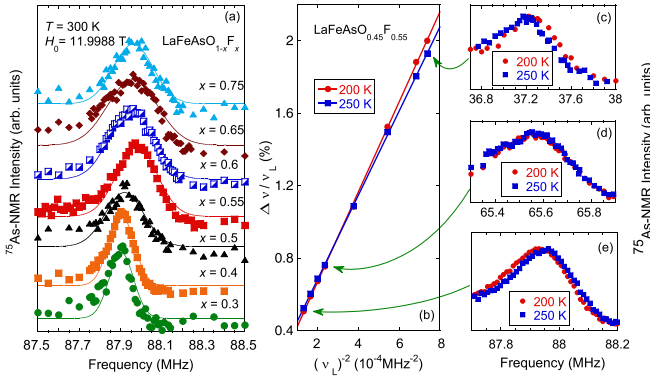


FIG. 3.  $^{75}\text{As}$  NMR spectroscopy and the procedure to obtain the quantity  $\nu_c \sqrt{1 + \frac{\eta^2}{9}}$ . (a)  $^{75}\text{As}$  NMR central transition peak with  $H_0 \parallel ab$ -plane for magnetically oriented powder. The peak corresponds to the central transition (the  $m = -1/2 \leftrightarrow 1/2$  transition). (b) An example of the plot of  $\Delta\nu/\nu_L$  against  $\nu_L^{-2}$  for different  $H_0$ . The quantities  $K$  and  $\nu_c^2(1 + \frac{\eta^2}{9})$  are obtained through the intersection with the vertical axis and the slope of the  $\Delta\nu/\nu_L$  versus  $\nu_L^{-2}$  line, respectively. (c-e) Demonstration of the NMR spectra at  $T = 200$  K and 250 K for three representative fields  $H_0 = 4.9983$  T, 8.9232 T and 11.9988 T.

new superconductivity dome and the symmetry-breaking structural phase transition boundary.

Below we elaborate how the C4 symmetry-breaking structural phase transition is identified. Taking advantage of the fact that the magnetic susceptibility in the  $ab$ -plane is larger than that along the  $c$ -axis[20], we obtain the  $^{75}\text{As}$  NMR spectra corresponding to  $H_0 \parallel a(b)$ -axis. Figure 3(a) shows the  $^{75}\text{As}$  NMR spectra of the magnetically-aligned grains under an applied magnetic field  $H_0 = 11.9988$  T. The total nuclear spin Hamiltonian is written as  $\mathcal{H} = \mathcal{H}_Z + \mathcal{H}_Q$ , where  $\mathcal{H}_Z = H_0(1 + K)$  is the Zeeman interaction with  $K$  being the Knight shift due to hyperfine interaction, and  $\mathcal{H}_Q = \frac{eV_{zz}Q}{4I(2I-1)}((3I_z^2 - I^2) + \frac{1}{2}\eta(I_+^2 + I_-^2))$  is due to the nuclear quadrupole interaction. The sizable  $\mathcal{H}_Q$  for  $^{75}\text{As}$  ( $I=3/2$ ) has a significant perturbation effect on the  $m = 1/2 \leftrightarrow -1/2$  transition (central transition), leading to a shift of this transition line. When a magnetic field is applied along the principal axis, say,  $z$ , the resonance frequency shift is given as [21],

$$\Delta\nu = \nu_{res} - \nu_L = K\gamma_N H_0 + \frac{(\nu_x - \nu_y)^2}{12(1+K)\nu_L} \quad (2)$$

Here  $\nu_L = \gamma_N H_0$  is the Larmor frequency and  $\nu_{res}$  is the observed resonance frequency. In undoped  $\text{LaFeAsO}$  at high temperature, the principal axes  $x, y, z$  coincide with the crystal  $a-, b-, c$ -axis [22].

When a four-fold symmetry is broken so that  $\eta$  is nonzero, the second term of the above equation becomes  $\frac{3\nu_c^2}{16(1+K)\nu_L}(1 - \frac{2}{3}\eta + \frac{\eta^2}{9})$  for  $H_0 \parallel a$ -axis, and it becomes  $\frac{3\nu_c^2}{16(1+K)\nu_L}(1 + \frac{2}{3}\eta + \frac{\eta^2}{9})$  for  $H_0 \parallel b$ -axis. Therefore, for

a twined single crystal or a magnetically-aligned powder sample, the averaged resonance frequency shift can be written as

$$\frac{3\nu_c^2}{16(1+K)\nu_L}(1 + \frac{\eta^2}{9}) \quad (3)$$

The quantity  $\nu_c \sqrt{1 + \frac{\eta^2}{9}}$  was obtained from the slop of the plot  $\Delta\nu/\nu_L$  against  $\nu_L^{-2}$  according to eq. (2) and (3). Figure 3(b-e) show an example of such procedure for the compound of  $x = 0.55$ .

Figure 4(a) shows the F-concentration dependence of the obtained  $\nu_c \sqrt{1 + \frac{\eta^2}{9}}$  at three representative temperatures. For all cases,  $\nu_c \sqrt{1 + \frac{\eta^2}{9}}$  changes progressively as F-content increases but shows a crossover at a certain F-concentration  $x_s$  that is temperature dependent. This result together with the fact that the lattice constant obtained by XRD also changes continuously as  $x$  increases [19] assure that the doping does increase with increasing  $x$ . Figure 4(b) shows the temperature dependence of  $\nu_c \sqrt{1 + \frac{\eta^2}{9}}$  for  $x = 0.3, 0.5$  and  $0.55$ . For the  $x = 0.3$  and  $0.5$  compounds, this quantity is temperature independent. By contrast, for  $x = 0.55$ , there is a clear transition taking place at a temperature between 250 and 200 K. The middle point of the transitions is defined as  $T_s$ . The  $x_s$  and  $T_s$  are plotted in Fig. 2(a). For  $x \geq 0.6$ , the above quantity is  $T$ -independent again below room temperature [19]. Since it has been established that  $\nu_c$  increases linearly with increasing doping [10] and decreases smoothly with decreasing temperature [19], the present results indicate that  $\eta$  undergoes an abrupt increase when crossing  $x_s$  or  $T_s$ . It is worthwhile pointing out that the  $T_s$  line extrapolates to absolute zero at  $x \sim 0.5$ , where the temperature dependence of the electrical resistivity shows a critical behavior of  $\rho - \rho_0 \propto T$ .

The abrupt change of  $\eta$  crossing  $x_s$  is further corroborated by the measurements at the La site. Figure 4(c) shows the  $^{139}\text{La}$  ( $I = 7/2$ ) NQR transition lines for  $x = 0.3$  and  $0.55$ . As seen in the inset to Fig. 4(c), the three transition lines are equally separated when  $\eta = 0$ . For finite  $\eta$ , however, the three lines are not equally separated; in particular, the lowest ( $m = \pm 1/2 \leftrightarrow \pm 3/2$ ) transition line largely shifts to a higher frequency as  $\eta$  increases. Such difference is exactly found between the  $x = 0.3$  and  $x = 0.55$  compounds. Our results reveal that  $\eta = 0$  for  $x = 0.3$  but  $\eta = 0.21$  for  $x = 0.55$ . Thus, above the new dome, there is a structural phase transition from a four fold symmetry at high temperature to a lower symmetry at low temperature.

Furthermore, we have directly confirmed the structural transition by Transmission Electron Microscope (TEM). Figure 5(a) shows the [001] zone-axis electron diffraction patterns for  $\text{LaFeAsO}_{0.45}\text{F}_{0.55}$  taken at  $T = 300$  K, which indicates that the crystal structure is tetragonal with the

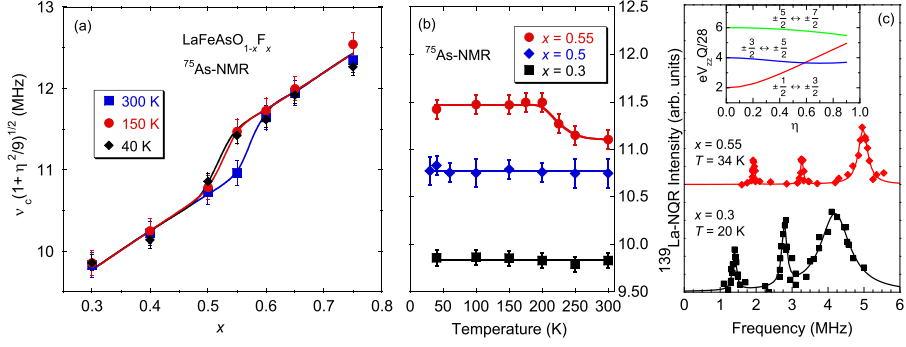


FIG. 4. Evidence for structural phase transition from electric field gradient tensors obtained by NMR and NQR. (a) The quantity  $\nu_c \sqrt{1 + \eta^2/9}$  plotted against fluorine content  $x$  at  $T=300, 150$  and  $40$  K. (b)  $\nu_c \sqrt{1 + \eta^2/9}$  as a function of temperature for  $x = 0.3, 0.5$  and  $0.55$ . The solid curves indicate the variation trend of the quantities. (c) The three  $^{139}\text{La}$ -NQR lines for  $x = 0.3$  are equally spaced, indicating  $\eta = 0$ , while those for  $x = 0.55$  are not, indicating a finite  $\eta$ . The inset shows the evolution of the three transition frequencies with increasing  $\eta$ .

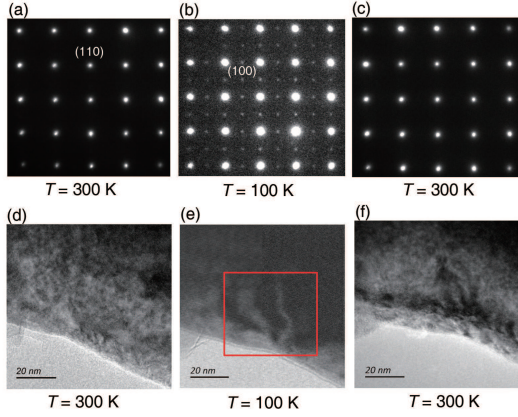


FIG. 5. Electron diffraction patterns of  $\text{LaFeAsO}_{0.45}\text{F}_{0.55}$  during a heat cycling of  $300$  K (a)  $\rightarrow$   $100$  K (b)  $\rightarrow$   $300$  K (c). Additional Bragg spots appear at the systematic (100) positions, indicating a change in crystal symmetry. (d-f) show the microstructures during the cycling. Domain structure appeared at  $T=100$  K as seen in the area marked by the red rectangle, but disappeared after heating back to  $300$  K.

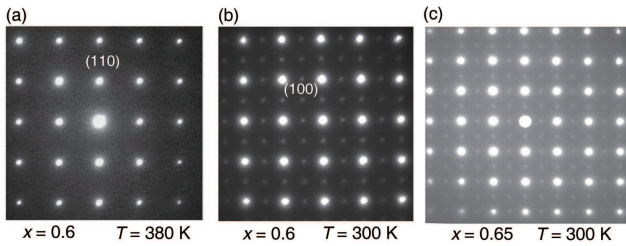


FIG. 6. Electron diffraction patterns of  $\text{LaFeAsO}_{0.4}\text{F}_{0.6}$  and  $\text{LaFeAsO}_{0.35}\text{F}_{0.65}$ . (a-b) TEM data for  $x = 0.6$  at  $T = 380$  K and  $300$  K. The images were taken along the  $[001]$  zone-axis direction. (c) The TEM image for  $x = 0.65$  at  $T = 300$  K. The crystal symmetry of this compound is also of orthorhombic already at room temperature.

space group of  $P4/nmm$ . At  $T = 100$  K, however, additional spots appear at (100) positions, as seen in Fig. 5(b). These features indicate unambiguously that the symmetry is lowered at low temperature. Furthermore, domain structures appear at low temperature as shown in Fig. 5(e) which are absent at  $T = 300$  K. These structures are due to twinning domains energetically preferred by structural relaxation following the phase transition.

Figure 5(a-c) shows the TEM results for  $x = 0.55$  during a heat cycling of  $300$  K  $\rightarrow$   $100$  K  $\rightarrow$   $300$  K, and (d-f) the corresponding microstructures. After cooling to  $100$  K and measuring the TEM images there, the sample was heated back to  $300$  K and measured again. We find that the tetragonal symmetry is recovered and the TEM data are reproducible. These results indicate that the additional spots and the domain structure found at  $T = 100$  K are intrinsic properties due to the structural transition. Around the structural phase transition temperature, we have taken TEM pictures in a step of  $5$  K and found no hysteresis during the heat cycling. It is noted that the observed changes both in the Bragg spots and in the microstructure agree completely with the cases of parent compounds  $\text{LaFeAsO}$  and  $\text{NdFeAsO}$  where a tetragonal-to-orthorhombic structural transition takes place at  $T_s = 135$  K [23]. Also, we have confirmed that the compounds with  $x=0$  and  $0.1$  synthesized under the same conditions as those for  $x \geq 0.3$  do have  $C4$  symmetry at room temperature, so the  $C4$  symmetry breaking below  $T_s$  for  $x > 0.5$  is not due to the high temperature and high pressure treatment.

Evidence for the structural transition was also obtained for  $x = 0.6$  as shown in Fig. 6(a-b). At  $T = 300$  K, the (100) spots and domain structures indicating  $C4$ -symmetry breaking was found. Upon heating from room temperature, the (100) spots disappeared at  $T = 380$  K. We therefore determined  $T_s = 380 \pm 5$  K for this composition and plotted this point in Fig. 2(a). Figure

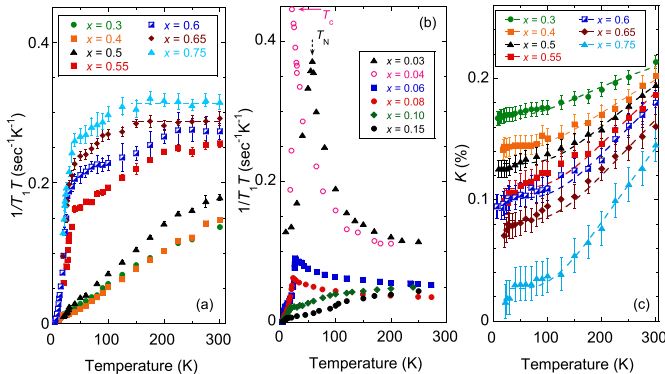


FIG. 7. The quantity  $1/T_1T$  and the Knight shift. (a) The variation of  $1/T_1T$  for  $x \geq 0.3$ . The broken lines show a  $1/T_1T = \text{const.}$  relation. (b) Data for  $x \leq 0.15$  taken from Ref. [10]. (c) The temperature dependence of the Knight shift  $K$  of  $H_0 \parallel ab$  for  $x \geq 0.3$ .

6(c) shows the TEM taken at  $T = 300$  K for  $x = 0.65$ . As for the  $x = 0.6$  compound discussed above, the C4 symmetry is also broken already at  $T = 300$  K for this composition. The TEM results are in agreement with the NMR data of  $T_s > 300$  K for  $x \geq 0.6$ .

The tetragonal-to-orthorhombic structural transition and the associated electronic nematicity (in-plane anisotropy) has been a main focus in the study of the mechanism for high- $T_c$  superconductivity in ironpnictides. In LaFeAsO or underdoped  $\text{BaFe}_{2-x}\text{M}_x\text{As}_2$  ( $\text{M} = \text{Ni}, \text{Co}$ ), a structural transition takes place above the magnetic order temperature  $T_N$  [6, 7, 24]. Below  $T_s$ , many physical properties exhibit nematic behavior [22, 25]. It has been proposed that the structural transition, the electronic nematicity, the magnetic transition and the superconductivity are inter-related [26].

Currently, there are two schools of theories. One is that the structural transition and the resulting electronic nematicity are directly driven by strong low-energy magnetic fluctuations [27]. However, our system is far away from a magnetic ordered phase, and there is no indication of low-energy magnetic fluctuations. Figure 7 (a) shows the temperature dependence of the quantity  $1/T_1T$ , with comparison to that for  $x \leq 0.15$  shown in Figure 7 (b) [10]. Figure 7 (c) shows the Knight shift  $K$  for the compounds of the new dome. For a conventional metal, both  $1/T_1T$  and  $K$  are temperature-independent. The first intriguing aspect seen from Fig. 7 (a) is that  $1/T_1T$  appears to fall into two groups, one for  $x \leq 0.5$  and the other for  $x > 0.5$ , which is consistent with the structural phase boundary shown in Fig. 2. Secondly, the two quantities  $1/T_1T$  and  $K$  for  $x \geq 0.3$  show a similar trend in the temperature variation; they decrease with decreasing temperature, suggesting that both of them are dominated by the density of states at the Fermi level. This is in sharp contrast to the low-doped compounds ( $x \leq 0.1$ )

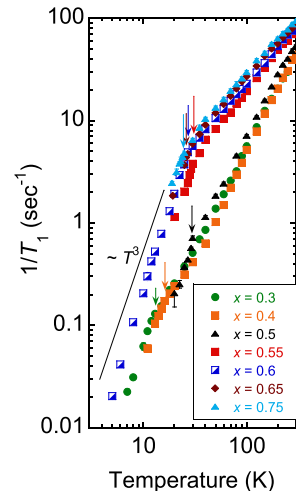


FIG. 8. The temperature dependence of the  $^{75}\text{As}$  spin-lattice relaxation rate  $1/T_1$ . The arrows indicate  $T_c$  under the magnetic field of  $H \sim 12$  T measured by the *insitu* NMR coil. The straight line is a guide to the eyes to indicate the  $1/T_1 \propto T^3$  relation.

where  $1/T_1T$  increases rapidly upon cooling [10, 28], due to the development of low-energy spin fluctuations. As can be seen in 7 (b), when there is a Neel order, as is the case for  $x = 0.03$ ,  $1/T_1T$  increases with decreasing temperature, forming a sharp peak at the Neel temperature  $T_N$ , due to a critical slowing down of the magnetic moments. When the magnetic order is suppressed by doping but magnetic (spin) fluctuations are present,  $1/T_1T$  follows a Curie-Weiss type of variation before superconductivity sets in [10], which is the case for  $x = 0.04, 0.06$  and  $0.08$ . However, non of these features are observed in the compounds of  $x \geq 0.3$ .

The second school of theories is that orbital order or fluctuations are responsible for the nematic structural transition and the superconductivity [29–33]. However, the proposed orbital fluctuations with finite momentum can be enhanced only when low-energy spin fluctuations exist [29, 31].

Thus, in the absence of low-energy spin fluctuations, the newly-discovered second dome with  $T_c$  even higher than the first dome, and the structural transition above  $T_c$ , pose a challenging issue. In this regard, the  $T$ -linear electrical resistivity seen around  $x_{opt}$  may provide a clue. Quantum fluctuations of an order parameter can lead to non-Fermi liquid behavior of the electrical resistivity [34]. In particular, a  $T$ -linear resistivity was often taken as a fingerprint of two-dimensional quantum magnetic fluctuations [35]. In the present case where low-energy magnetic fluctuations are absent, it is tempted to consider that the observed  $T$ -linear resistivity is caused by the fluctuations of widely-searched electronic nematic order such as orbital order. In fact, a similar  $T$ -linear resistivity

was found in  $\text{BaFe}_{2-x}\text{Ni}_x\text{As}_2$  ( $x=0.14$ ) which is far away from the magnetic quantum critical point ( $x=0.10$ ) and  $T_s$  extrapolates to zero there [7]. To our knowledge, the temperature dependence of the electrical resistivity due to orbital fluctuations has not been theoretically worked out yet. Our work indicates that exploring the origin of the  $T$ -linear electrical resistivity is an important task since the issue may further be related to the driving force of the structural transition as well as to the mechanism of superconductivity in the whole iron-pnictides family. Also, future study of the nematicity in the physical properties for this system will greatly help move the research field further ahead.

Finally, we briefly touch on the properties of the superconducting state. Figure 8 shows the temperature dependence of the spin-lattice relaxation rate  $1/T_1$  for the new dome. For all F-concentrations, there is a clear and sharp decrease below  $T_c$ , which assures the bulk nature of the superconductivity. The detailed temperature variation below  $T_c$  seems to be similar between  $x = 0.6$  in the new dome and  $x = 0.08$  in the first dome [19].

Before closing, we emphasize that the phase diagram discovered here resembles that of heavy fermion compound  $\text{CePd}_2\text{Si}_2$  where a  $T$ -linear resistivity was also found at the top of the dome [2]. However, the  $T_N$  line in  $\text{CePd}_2\text{Si}_2$  is replaced by  $T_s$  line in our case. Therefore, the new superconductivity dome reported here may represent a new paradigm of superconductivity. Our finding may also shed light on the physics of heavy fermion materials such as  $\text{CeCu}_2\text{Si}_2$  where two superconducting phases, one close to magnetism and the other far away from magnetism, were reported [36]. In the context of iron pnictides, the heavily F-doped  $\text{LaFeAsO}_{1-x}\text{F}_x$  system made by the high-pressure synthesis technique also represents a unprecedented class of superconductors. Previously, hydrogen substitution for oxygen up to 53% was reported to dope electron efficiently and induce two superconducting regions that merge into one at high pressure [17]. However, all the superconducting regions there have a tetragonal crystal structure with C4 symmetry and the superconducting phase at the high-doping region is in close proximity to an adjacent magnetic ordered phase at  $x \geq 0.53$  [37].

In conclusion, we have reported the discovery of a new superconductivity dome without low-energy magnetic fluctuations in  $\text{LaFeAsO}_{1-x}\text{F}_x$  with  $0.25 \leq x \leq 0.75$ , where the maximal critical temperature  $T_c$  at  $x_{opt} = 0.5 \sim 0.55$  is even higher than that at  $x \leq 0.2$ . By nuclear magnetic resonance and Transmission Electron Microscopy, we demonstrated that a C4 rotation symmetry-breaking structural transition takes place for  $x > 0.5$  above  $T_c$ . Our results point to a new paradigm of high temperature superconductivity, and suggest that there may be a new route to high temperature superconductivity and that superconductors with further higher  $T_c$

await discovery.

We thank Z. Li for assistance in some of the measurements, T. Xiang, L. L. Sun, S. Onari, H. Ikeda and H. Kontani for helpful discussion. This work was partially supported by CAS's Strategic Priority Research Program, No. XDB07020200, National Basic Research Program of China, Nos. 2012CB821402, 2011CBA00109 and 2011CBA00101, and by NSFC Grant No 11204362.

---

\* gqzheng123@gmail.com

- [1] Lee P A, Nagaosa N, Wen X G 2006 *Rev. Mod. Phys.* **78** 17
- [2] Mathur N D *et al.* 1998 *Nature* **394** 39
- [3] Kamihara Y, Watanabe T, Hirano M, Hosono H 2008 *J. Am. Chem. Soc.* **130** 3296
- [4] Ren Z A *et al.* 2008 *Chin. Phys. Lett.* **25** 2215
- [5] Rotter M, Tegel M, Johrendt D 2008 *Phys. Rev. Lett.* **101** 107006
- [6] Sefat A S *et al.* 2008 *Phys. Rev. Lett.* **101** 117004
- [7] Zhou R *et al.* 2013 *Nat. Commun.* **4** 2265
- [8] Ren Z A *et al.* 2008 *EPL* **83** 17002
- [9] Ning F L *et al.* 2010 *Phys. Rev. Lett.* **104** 037001
- [10] Oka T *et al.* 2012 *Phys. Rev. Lett.* **108** 047001
- [11] Li Z *et al.* 2011 *Phys. Rev. B* **83** 140506(R)
- [12] Mazin I I, Singh D J, Johannes M D, Du M H 2008 *Phys. Rev. Lett.* **101** 057003
- [13] Kuroki K *et al.* 2008 *Phys. Rev. Lett.* **101** 087004
- [14] Graser S *et al.* 2010 *Phys. Rev. B* **81** 214503
- [15] Luetkens H *et al.* 2009 *Nat. Mater.* **8** 305
- [16] Lu W *et al.* 2008 *Solid State Commun.* **148** 168
- [17] Iimura S *et al.* 2012 *Nat. Commun.* **3** 943
- [18] Narath A 1967 *Phys. Rev.* **162** 320
- [19] More data will be presented in a separate paper.
- [20] Matano K *et al.* 2008 *EPL* **83** 57001
- [21] Abragam A *The Principles of Nuclear Magnetism* (Oxford University Press, London, 1961).
- [22] Fu M *et al.* 2012 *Phys. Rev. Lett.* **109** 247001
- [23] Ma C *et al.* 2008 *EPL* **84** 47002
- [24] de la Cruz C *et al.* 2008 *Nature* **453** 899
- [25] Chu J H *et al.* 2010 *Science* **329** 824
- [26] Fernandes R M, Chubukov A V, Schmalian J. 2014 *Nat. Phys.* **10** 97
- [27] Fernandes R M, Bohmer A E, Meingast C, Schmalian J 2013 *Phys. Rev. Lett.* **111** 137001
- [28] Nakai Y, Kitagawa S, Ishida K 2009 *New J. Phys.* **11** 045004
- [29] Kontani H, Onari S 2010 *Phys. Rev. Lett.* **104** 157001
- [30] Chen C C *et al.* 2010 *Phys. Rev. B* **82** 100504
- [31] Lee C C, Yin W G, Ku W 2009 *Phys. Rev. Lett.* **103** 267001
- [32] Lv W C, Wu J S, Phillips P 2009 *Phys. Rev. B* **80** 224506
- [33] Yamase H, Zeyher R 2013 *Phys. Rev. B* **88** 180502(R)
- [34] Hertz J A 1976 *Phys. Rev. B* **14** 1165
- [35] Moriya T 1991 *J. Mag. Mat.* **100** 261
- [36] Yuan H Q *et al.* 2003 *Science* **302** 2104
- [37] Hiraishi M *et al.* 2014 *Nat. Phys.* **10** 300